npj | quantum materials

Article

Published in partnership with Nanjing University

https://doi.org/10.1038/s41535-025-00755-6

A magnon band analysis of $GdRu_2Si_2$ in the field-polarized state

Check for updates

G. D. A. Wood[1,2] ✉, J. R. Stewart[2], D. A. Mayoh[1], J. A. M. Paddison[3], J. Bouaziz[4], S. M. Tobin[5,6], O. A. Petrenko[1], M. R. Lees[1], P. Manuel[2], J. B. Staunton[1] & G. Balakrishnan[1] ✉

Understanding the formation of skyrmions in centrosymmetric materials is a problem of fundamental and technological interest. $GdRu_2Si_2$ is a candidate material that hosts a variety of multi-Q magnetic phases, including in zero-field. Here, inelastic neutron scattering is used to measure the spin excitations in the field-polarized phase of $GdRu_2Si_2$. Linear spin wave theory and a method of interaction invariant path analysis are used to derive a Hamiltonian accounting for the spectra. The Hamiltonian, dominated by bilinear (Ruderman-Kittel-Kasuya-Yosida) Heisenberg exchange, compares favorably to ab initio calculations. Dipolar interactions are a secondary energy scale to consider, with $J_{\mathrm{D.D}} \sim 0.05 J_{\mathrm{RKKY}}$. However, it is shown that in the field-polarized phase the dipolar interactions 'self screen' so that their effect is largely suppressed. No specific evidence for higher-order exchange is found. These aspects are discussed in the context of the lower field multi-Q states and the anisotropy of the system.

Materials with topologically protected properties are expected to prevail in the next generation of electronics[1]. Magnetic skyrmions are a prominent area of research within this field as these vortexlike spin configurations feature remarkable properties, including field-driven skyrmion motion, the topological Hall effect, and non-reciprocal response, which may find applications in spintronics[2–4]. Understanding how skyrmions may form in ambient conditions is a key challenge in the drive to discover technologically significant materials. In this regard, centrosymmetric systems are an important class of materials as, in principle, it has been shown that skyrmions may be stabilized in zero-field[5,6], and may also exhibit novel properties such as non-fixed helicity[7–9].

A number of centrosymmetric skyrmion candidates based on Gd^{3+} and Eu^{2+} intermetallics have been experimentally identified; magnetic ions with weak anisotropy are an important attribute for skyrmion spin-textures. These materials include Gd_2PdSi_3[10–12], $Gd_3Ru_4Al_{12}$[13,14], $GdRu_2Si_2$[15–21], $GdRu_2Ge_2$[22], $EuAl_4$[23–27] and $EuAl_xGa_{2-x}$[28–30]. The latter four systems form in the widely studied $ThCr_2Si_2$-type parent structure. Aside from the diverse range of emergent physics originating from this structure-type[31], the broad chemical tunability of this simple structure makes appealing grounds for theoretical and material discovery initiatives[32]. Putatively, in these materials, the Fermi surface topography and, in turn, long-ranged Ruderman-Kittel-Kasuya-Yosida (RKKY) interactions act to form the multi-Q spin structures[33]. However, there are several differences between the phase diagrams and magnetic structures of each material. This is most clear in the case of $GdRu_2Si_2$, which, unlike the other candidates, has a multi-Q incommensurate ground state in zero field, which is a highly unusual property[19,34,35]. Hence, understanding how the ground state of $GdRu_2Si_2$ forms may provide evidence as to how zero-field skyrmions may be realized. For systems with one magnetic site per primitive unit cell, a key implication of zero-field multi-Q states is the inclusion of anisotropic or higher-order exchange terms in the Hamiltonian (such as biquadratic or four-spin interactions), as the Luttinger-Tisza method stipulates that models with only bilinear Heisenberg exchange terms stabilize single-Q structures[36–38]. A second unresolved aspect of magnetism in $GdRu_2Si_2$ is the large degree of anisotropy between H-T phase diagrams for different directions of applied field[18,39]. Naturally, this would imply single-ion anisotropy or anisotropic bilinear exchange interactions entering the Hamiltonian. However, these terms ordinarily arise due to spin-orbit coupling, which ostensibly in an $S = 7/2$, $L = 0$ system is not present.

In view of gauging the magnetic interactions in $GdRu_2Si_2$, inelastic neutron scattering measurements of excitations frequently provide stringent and comprehensive tests of magnetic models. However, the application of this method to incommensurate order is in general limited; the magnetic Brillouin zone is very confined and there are a large number of excitation bands, so that there are many closely spaced excitations beyond the resolution capabilities of modern spectrometers[40–42]. Nevertheless, studying

[1]Department of Physics, University of Warwick, Coventry, UK. [2]ISIS Facility, STFC Rutherford Appleton Laboratory, Harwell Science and Innovation Campus, Oxfordshire, UK. [3]Neutron Scattering Division, Oak Ridge National Laboratory, Oak Ridge, TN, USA. [4]Peter Grünberg Institut and Institute for Advanced Simulation, Forschungszentrum Jülich & JARA, Jülich, Germany. [5]Clarendon Laboratory, Department of Physics, University of Oxford, Oxford, UK. [6]Australian Nuclear Science and Technology Organisation, Lucas Heights, NSW, Australia. ✉e-mail: george.wood@stfc.ac.uk; g.balakrishnan@warwick.ac.uk

various magnets in the simplified case of the field-polarized phase frequently proves to be an effective method to gain insights into the key magnetic interactions of a system[43,44].

In this paper, the spin waves of $GdRu_2Si_2$ in the field-polarized state are examined using inelastic neutron scattering. Analysis of the magnon band is implemented using linear spin wave theory and a method of interaction invariant path analysis. The spectra are accounted for using a set of bilinear Heisenberg exchange interactions up to the eighth nearest neighbor, indicative of the long-range RKKY interactions. Qualitatively, the model agrees well with ab initio calculations[33]. Following this, the effect of dipolar interactions on the magnon dispersion is investigated. It is shown that in the field-polarized phase, the dipolar interactions 'self-screen' so that their effect is suppressed. However, it is argued that in the non-collinear phases, this 'self-screening' may not necessarily occur, and in this case, dipolar interactions are a secondary energy scale to consider, with $J_{\mathrm{D.D}} \sim 0.05 J_{\mathrm{RKKY}}$. Higher-order exchange interactions are not required to model the excitation spectra. The implications of the derived Hamiltonian are discussed within the context of the multi-Q phases and anisotropic phase diagrams of $GdRu_2Si_2$.

Analysis

An overview of the inelastic neutron spectra is provided in Fig. 1. The observation of a single band is consistent with Gd^{3+} being the only magnetic ion within the primitive unit cell. In addition to the magnon band, there are several low-energy spurious signals originating from the sample environment (e.g., Fig. 1a at $\hbar\omega$ ~0.8 meV), which, since the excitation signal from the sample is intrinsically low due to the absorption, appear comparatively strong. So that the magnon band signal could be systematically extracted, median kernel filtering was applied; this methodology is described in detail in the Supplementary Note 1.

To model the magnon band, we start by assuming a Hamiltonian with bilinear Heisenberg exchange, Zeeman coupling, and single-ion anisotropy,

$$H = \sum_{i,j} \left\{ J_{i,j} \mathbf{S}_i \cdot \mathbf{S}_j \right\} + \sum_i \left\{ g\mu_{\mathrm{B}} \mathbf{B} \cdot \mathbf{S}_i + K\left(S_i^z\right)^2 \right\}. \quad (1)$$

Applying the Holstein-Primakoff transformation provides the linear spin-wave dispersion for a ferromagnet,

$$\hbar\omega(\mathbf{q}) = S[J(\mathbf{q}) - J(\mathbf{0})] - g\mu_{\mathrm{B}} B - 2KS, \quad (2)$$

where $J(\mathbf{q})$ is defined as,

$$J(\mathbf{q}) = \sum_{\boldsymbol{\delta} \neq 0} J_{\boldsymbol{\delta}} \exp(i\mathbf{q} \cdot \boldsymbol{\delta}). \quad (3)$$

Here, $\boldsymbol{\delta}$ is the interaction vector $(\mathbf{r}_i - \mathbf{r}_j)$ between the magnetic ions expressed in lattice units, and $\mathbf{q}$ is a reciprocal space vector (in r.l.u.)[45]. Note, that with the experiment taking place at approximately half of the ordering temperature, we have considered the effects of interaction renormalization due to finite temperature. We have calculated, following the Hartree-Fock approximation, as set out in Lovesey[46], that the renormalization is in a Q-independent regime, and that the rescaling of the interactions is limited to $\lesssim$4%, such that it does not qualitatively affect the interpretation of the results, and that linear spin wave theory is appropriate to model the excitations. All of this indicates that higher-order magnon processes are not prevalent throughout the system at 25 K, and this is corroborated by the fact that the dispersion is characteristically sharp within our instrumental resolution. Initial attempts at fitting the magnon dispersion revealed that J_2 (with $\boldsymbol{\delta}$ = [1/2, 1/2, 1/2]) is the dominant interaction, but that multiple

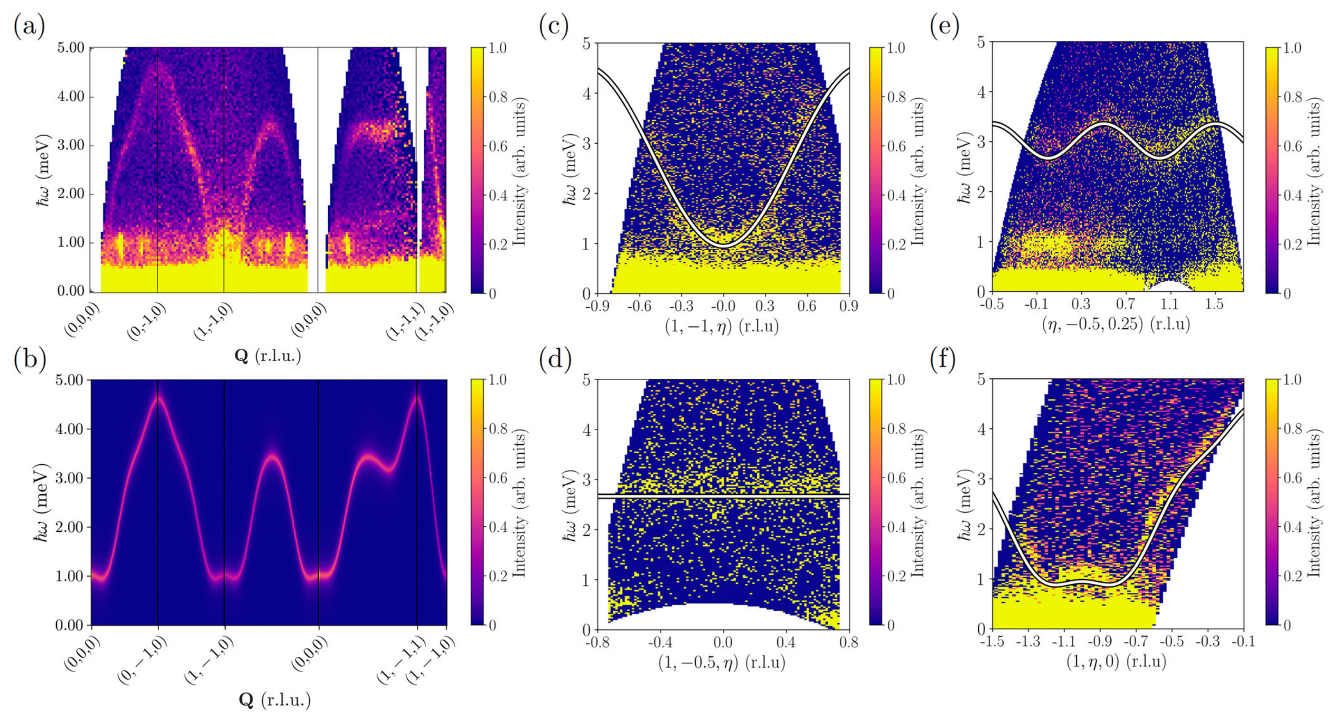

Fig. 1 | Various momentum-resolved inelastic neutron scattering spectra of $GdRu_2Si_2$ at T = 25 K and B = 8.8 T in the field-polarized phase (E_i = 7.52 meV). A single magnon band is observed throughout. **a** An overview of the inelastic neutron scattering data. **b** Corresponding calculation of the magnon dispersion model implemented in the *Su(n)ny* code[48,49]. **c** An out-of-plane magnon dispersion along the $(1, -1, \eta)$ path. J_2 is active and dominant along this cut. **d** A J_2 invariant cut on the $(1, -0.5, \eta)$ path; a flat band is observed and this indicates J_7 is negligible. **e** A J_2 invariant cut along the $(\eta, -0.5, 0.25)$ path; the magnon band is dispersive and therefore several in-plane interactions are required in the model. **f** A cut along $(1, \eta, 0)$, which passes directly over a zone center $(1, -1, 0)$. The '*w*' shape at the bottom of the dispersion curve is indicative of the incommensurate order stabilized at lower fields. In (**c**–**f**) the white/black line superimposed on the data is calculated using the spin-wave model described in the text. The complete set of cuts used for fitting the linear spin wave model is shown in Supplementary Note 2 (Figs. S2, S3, and S4).

interactions were required to account for the dispersion character, consistent with long-ranged RKKY interactions. To gauge which interactions are active in the system we have developed a method of interaction invariant path analysis. In this technique, reciprocal space cuts of $S(\mathbf{Q}, \omega)$ are chosen so that a specified interaction is inactive; i.e., the spin-wave theory pertaining to the interaction is non-dispersive along the reciprocal-space path. By isolating certain interactions, weaker, but nevertheless significant exchange interactions may be refined. In particular, we make use of J_2 invariant paths. The linear spin wave theory for the J_2 interaction is given by,

$$\hbar\omega(\mathbf{q}) = 8SJ_2\{\cos(\pi q_x)\cos(\pi q_y)\cos(\pi q_z) - 1\}. \tag{4}$$

Cancellation of the cosine terms in Eq. (4) is provided when q_x, q_y or $q_z = 1/2$ so that the J_2 term will only manifest as a constant in the dispersion relation. For instance, consider the $(1, -1, \eta)$ cut shown in Fig. 1c. A strong parabolic dispersion dominated by the J_2 interaction is evident. Conversely, the $(1, -0.5, \eta)$ cut in Fig. 1d is a J_2 invariant cut with $q_y = -1/2$. This invariant path is effective for constraining out-of-plane interactions, such as J_7 ($\boldsymbol{\delta} = [0, 0, 1]$). Since a flat band is observed this implies that J_7 is negligible, and therefore it is not included as a parameter in the model. Similarly, the $(\eta, -0.5, 0.25)$ cut of Fig. 1e is a J_2 invariant, and this path is effective for constraining interactions with $\boldsymbol{\delta} = [r_x, r_y, r_z = 0]$, which includes J_1 and J_3 (see Table 1). Since the magnon band along this path is dispersive, these parameters are included in the model. Additional notes for this new methodology are provided in the Supplementary Note 3.

The measurement did not contain sufficient intensity to reliably fit $S(\mathbf{Q}, \omega)$; hence, an $\hbar\omega(\mathbf{q})$ fitting was implemented instead using a least-squares minimization routine with the *LMFIT* package[47]. In total, seven bilinear Heisenberg exchange interactions and a constant parameter (C) were used to fit the magnon band (see Table 1). We define $B = -8.8$ T with the field applied along the z direction in this model. Only including J_1 to J_5 resulted in dispersions with global minima coinciding with zone centers, which would be consistent with an intrinsic ferromagnet. With a J_1 to J_6 model, the dispersion relation adopted global minima surrounding the zone center at incommensurate positions, but these minima were along the [1, 1, 0] direction, which would be inconsistent with the direction of the magnetic propagation in the lower-field phases. By including a J_8 interaction, the dispersion relation adopts global minima at $\mathbf{q} = [0.15, 0, 0]$, which is the correct direction for magnetic propagation. Conceivably, if the magnetic field was lowered, then the magnon band would lower, and where the minima coincide with $\hbar\omega = 0$ a field-polarized → incommensurate phase transition would take place. Models including further exchange interactions were found to marginally increase the quality of the fit; however, this came at the expense of higher correlation between parameters. With a preference for a minimal effective model that captures the salient features of the spin-wave dispersion, the J_1 to J_8 ($J_{1\to8}$) model suffices. The constant term in the model was refined to $C = 0.94 \pm 0.01$ meV. Noting that $-g\mu_B B = 1.02$ meV, we consider the refined value C to be broadly consistent with $-g\mu_B B$ when demagnetization effects would be expected to slightly lower the contribution of the field. Implicitly, from Eq. (2), it is not possible to disentangle constant contributions to the dispersion relation; i.e., $-g\mu_B B$, $-2KS$, and any unaccounted interaction terms. Indeed, depending on the number of exchange terms included in the model, the refined value of C varied between 0.88 ~ 0.99 meV, generally increasing with the number of exchange terms included. Therefore, we attribute the difference $\delta = -g\mu_B B - C$ as likely arising from small unaccounted exchange terms, and consider C to be consistent with that of the applied magnetic field with negligible single-ion anisotropy in the Hamiltonian.

Table 1 | A list of bilinear Heisenberg interactions and the experimentally derived interaction energies of the $J_{1\to8}$ model

Interaction (μeV)	δ	Multiplicity
$J_1 = -33.9 \pm 1.0$	[1, 0, 0]	4
$J_2 = -65.1 \pm 0.7$	[1/2, 1/2, 1/2]	8
$J_3 = 13.6 \pm 0.7$	[1, 1, 0]	4
$J_4 = -1.1 \pm 0.4$	[3/2, 1/2, 1/2]	16
$J_5 = 10.8 \pm 0.8$	[2, 0, 0]	4
$J_6 = 6.0 \pm 0.5$	[1, 2, 0]	8
$J_7 = 0$	[0, 0, 1]	2
$J_8 = 3.0 \pm 0.4$	[3/2, 3/2, 1/2]	8

$\boldsymbol{\delta}$ is the vector in lattice units over which each interaction acts (not including symmetry equivalents). The multiplicity of the interaction counts symmetry equivalent $\boldsymbol{\delta}$ vectors for each interaction.

We also evaluate the effect of dipolar interactions within the system. The Hamiltonian for a pairwise dipolar interaction is given by,

$$H_{\mathrm{D.D}} = \frac{\mu_0}{4\pi r^3}\left[\boldsymbol{\mu}_a \cdot \boldsymbol{\mu}_b - 3(\boldsymbol{\mu}_a \cdot \hat{\mathbf{r}})(\boldsymbol{\mu}_b \cdot \hat{\mathbf{r}})\right]. \tag{5}$$

Here $\boldsymbol{\mu}_{a,b}$ denotes a magnetic moment on a given site (a or b), and $\mathbf{r}$ is the vector between these sites. An approximate energy scale for these interactions can be ascertained from the nearest neighbor (nn) interaction as $H_{\mathrm{D.D,(nn)}} \sim 0.4$ K. This can be compared to the largest RKKY interaction $J_2S^2 \sim 8.8$ K. Given that both the dipolar and RKKY interactions decay as r^{-3}, it is reasonable to estimate that the dipolar interactions act at approximately 5% of the RKKY energy scale ($J_{\mathrm{D.D}} \sim 0.05 J_{\mathrm{RKKY}}$). This indicates that although the dipolar interactions are small, they are not irrelevant. Following this we calculate the effect of dipolar interactions on the spin-wave model of the system. These calculations were implemented with Ewald summation using the *Su(n)ny* code[48,49] and are presented in Fig. S6 of Supplementary Note 4. We find that in the field-polarized phase, the dipolar interactions have an almost imperceptible effect on the spin-wave calculations. On further investigation, it appears that in the field-polarized phase of this system, the dipolar interactions largely 'self-screen' each other[50,51]. For instance, in performing truncated calculations it is apparent that the most significant nearest neighbor and next nearest neighbor dipolar interactions almost perfectly cancel each other out in the dispersion relation. Therefore, it is clear that in the field-polarized phase dipolar interactions are of limited relevance. However, where the magnetic structure is non-collinear, this may not be the case; the second term in Eq. (5) will project more frequently, and this is a pathway through which momentum-dependent anisotropic exchange interactions may enter the Hamiltonian[17].

Discussion

A comparison between the ab initio model derived by Bouaziz et al.,[33] and the $J_{1\to8}$ model is shown in Fig. 2. In most aspects it is clear that both models are qualitatively consistent and there is a remarkable likeness between the dispersion shapes which substantiates the veracity of the ab initio calculations by Bouaziz et al.[33] This conclusion is consistent with the recent zero-field powder study of $GdRu_2Si_2$ by Paddison et al.[52]. From Fig. 2a, the two main points of difference between the models are at the top and bottom of the dispersions. The maximum of the dispersion model of Bouaziz et al. underestimates the measured magnon band and does not fit the data. However, at the bottom of the band, the model of Bouaziz et al. is likely more representative of the underlying incommensurate physics than the $J_{1\to8}$ model. This is since the global minimum of the ab initio model is at (0.18, 0, 0), which is closer to the magnetic propagation vector of $\mathbf{q}_e = [0.22, 0, 0]$ as determined by high-resolution diffraction experiments[15,18,19,52]. Likely, the reason the location of the global minimum of the $J_{1\to8}$ model is substantially less than $|\mathbf{q}_e|$ is since the bottom of the magnon band is not directly resolvable in the measurement, as the strong tail of elastic scattering obscures these details for $\hbar\omega < 0.8$ meV (see Fig. 1f). Without this information, the determination of the global minimum of the magnon band is somewhat uncertain, and the fitted model can only infer these minima from higher energy portions of the measured dispersion relation. Following this, given that at 25 K the system enters the field-polarized phase at 7.36 T, then with the applied magnetic field of 8.8 T, we would estimate that the bottom of the dispersion curve should sit at $-g\mu_B\Delta B \approx 0.17$ meV. Again, the minimum of

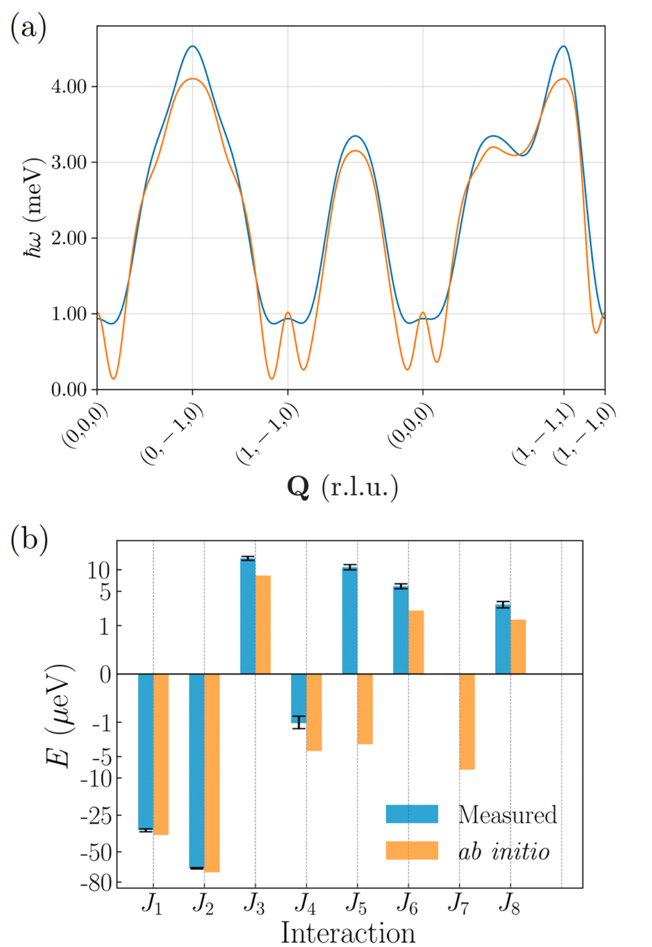

Fig. 2 | Comparisons between the experimentally derived effective model and the ab initio model derived by Bouaziz et al.[33]. a The dispersion of the ab initio model[33] (using J_1 to J_{50}) is represented by the orange line and the $J_{1\rightarrow 8}$ effective model is represented by the blue line. **b** Comparison of the experimentally determined Heisenberg exchange terms in $GdRu_2Si_2$ with those of the ab initio model[33]. Note that a cube root scale is used along the y axis for approximate RKKY scaling ($J_{\mathrm{RKKY}} \sim r^{-3}$).

the dispersion for the model of Bouaziz et al. is closer to this calculation. With regards to the $J_{1\rightarrow 8}$ model we adduce that additional exchange interactions would be required to recover more realistic global minima in the dispersion relation. Indeed, this was a key aspect of the model derived by Bouaziz et al., which found that a long-range *tail* of RKKY interactions had to extend up to ten unit cells[33]; the point being, that it was the cumulative effect of these weak interactions which was central in determining a propagation vector in reasonable agreement with experiment. However, without directly measuring the bottom of the magnon band below $\hbar\omega <$ 0.8 meV it is not possible to fit more interactions, and in any case, fitting a long-range *tail* of interactions within ten unit cells would introduce an intractable number of parameters. Supposing that there are unaccounted interactions in the $J_{1\rightarrow 8}$ model, we calculate a mean-field estimation of the Curie-Weiss temperature for the model: $\Theta = -\frac{S(S+1)}{3}J(\mathbf{0}) = 30.5\,\mathrm{K}$. Comparing this to the experimental value of 42.3 K (see Supplementary Note 5: Fig. S7) indicates that our model accounts for 72% of net ferromagnetic interactions in the system. This conclusion is corroborated by Fig. 1d which shows that the flat-band is slightly underestimated in the spin-wave model. Finally, Fig. 2b directly compares the values of the exchange terms in both models. There is very good agreement between exchange values for the first few parameters, but there is clear departure between the models for J_5 and J_7. The omission of J_7 in the effective model has been motivated by the flat band in Fig. 1d. The reason that J_5 is required to be antiferromagnetic in the $J_{1\rightarrow 8}$ model is so that the global minimum of the band lies at incommensurate positions; this particular difference between the ab initio model of Bouaziz et al., is likely due to not including the long-range exchange parameters ($J_{n>8}$) in the effective model.

More generally, the model Hamiltonian can be considered in the context of the lower-field multi-Q states and the anisotropy in the phase diagrams[19,39]. We have determined that the magnon band is dominated by a set of bilinear (RKKY) Heisenberg interactions. Crucially, to model the magnon band, higher-order exchange interactions are not required. This is consistent with the calculations of Bouaziz et al.[33] which found negligible evidence for these types of interactions. We have discussed that dipolar interactions, as an intrinsic source of anisotropic exchange, may be an important secondary energy scale to consider in this system[17]. Indeed this could have significant physical consequences as anisotropic exchange interactions can, in principle, induce multi-Q magnetic structures without a magnetic field[50]. In addition, they also couple the spins to the anisotropy of the lattice, and, therefore may be an important consideration for the anisotropic phase diagrams. Aside from these aspects, another form of anisotropy could arise from the RKKY interaction and the Fermi-surface topography. The RKKY interaction develops as a feedback effect between valence electrons at the Fermi surface and the order on the localized $4f$ magnetic moments. Tacitly then, it is a function of both temperature and magnetic field (i.e., $J_{i,j}$ ($\mathbf{B}$, T)), as through Neumann's principle the C_4 symmetry of the system will be broken (or preserved) according to the direction of the applied field, which should manifest in the Fermi surface topography and RKKY potential. The notion of an evolving Fermi surface between magnetic phases in this system is consistent with the nesting conditions which have been identified in angle-resolved photoemission spectroscopy studies[53,54] and the quantum oscillations study of Matsuyama et al., that associated a Fermi surface reconstruction with a change in oscillation frequency in measurements between the field-polarized and lower-field multi-Q state[55]. One final feature of the multi-Q phases to consider, is the intricate coupling between magnetic and charge density wave order. In the field-polarized phase of $GdRu_2Si_2$ it has been shown that charge density waves do not exist, whereas in the multi-Q phases concomitant charge density waves propagate at even harmonics of the magnetic propagation[16]. Currently, the precise details of the symmetry breaking of the spin-lattice distortions are not fully understood. Irrespective of these details, the incommensurate charge density will act to modulate the Heisenberg exchange network across the system. In some cases, this can give rise to more complex magnetic ordering in zero magnetic field[56,57]. Experiments which are able to determine the nature of the charge density wave symmetry breaking in these types of systems are certainly of future interest[58,59].

In conclusion, a magnon band in the field-polarized phase of $GdRu_2Si_2$ has been measured using time-of-flight inelastic neutron scattering. A Hamiltonian accounting for the dispersion relation has been derived with linear spin wave theory. The model, using eight free parameters, is in good accordance with ab initio calculations[33], and captures the salient features of the magnon dispersion, including global minima at incommensurate positions, which are characteristic of the lower-field magnetism. There are a few indications that more exchange interactions are present in the system, with the cumulative effect of long-range RKKY interactions being significant. However, we do not find any specific evidence for higher-order exchange interactions. We have shown that in the field-polarized phase, dipolar interactions act to 'self-screen' each other. At lower fields with non-collinear magnetic structures, we posit that this may not be the case[17], and hence dipolar interactions are a secondary energy scale to consider with $J_{\mathrm{D.D}} \sim 0.05 J_{\mathrm{RKKY}}$. Conceivably, the introduction of these anisotropic terms in the Hamiltonian could lift degeneracies between single and multi-Q magnetic structures. This conclusion may well have implications for other $S = 7/2$, $L = 0$ centrosymmetric skyrmion intermetallics, which frequently have lower ordering temperatures, and therefore, presumably the dipolar interactions are an even more relevant energy scale[27]. We have also highlighted the role of spin-lattice distortions in this system[16] and an evolving

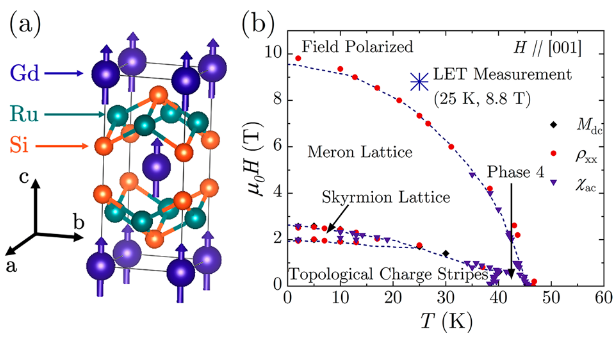

Fig. 3 | Structure and phase diagram of $GdRu_2Si_2$. **a** Conventional unit cell of $GdRu_2Si_2$, which forms in the *I*4/*mmm* space group (with $a = 4.16$ Å and $c = 9.59$ Å) with the Gd moments depicted in a field-polarized state. **b** *H*-*T* phase diagram of $GdRu_2Si_2$ with *H* applied along the *c* axis. The position of the LET *Horace* scan is marked at (25 K, 8.8 T).

Fermi-surface as a function of applied field-direction and temperature[55]. Future experimental efforts will focus on investigating the coupling between magnetic and charge density wave order so that the origin of the multi-Q zero-field ordering may be understood.

Methods

To enable neutron scattering, 98.1% isotopically enriched ^{160}Gd was used. The $^{160}GdRu_2Si_2$ single crystal boule, 17 mm in length and ~2.3 mm in diameter, the same as that used in ref. 19, was mounted on an aluminum strip holder. Single-crystal inelastic neutron scattering measurements were performed on the LET spectrometer (a direct geometry time-of-flight instrument) at the ISIS Neutron and Muon Source[60]. Measurements were taken at 25 K with an 8.8 T magnetic field applied along the *c* axis so that the sample was in the forced ferromagnetic state (see Fig. 3) with a^*-b^* as the primary scattering plane. A principal incident energy of $E_i = 7.52$ meV was used with a percentage resolution of 3.7% at the elastic line. With the multiplexing capability of LET, three other incident energies were available ($E_i = 2.2$, 3.7 and 22.80 meV). The two lower incident energies would have been useful for resolving the dispersion at the lowest energies. However, the absorption of the sample at these lower energies was more severe and no magnon signal was perceptible. Note that despite the ^{160}Gd enrichment, the sample is very absorbing with $\bar{\sigma}_a(E_i = 7.52\,\mathrm{meV}) \approx 1736\,\mathrm{b}$ and hence the signal-to-noise ratio of the measurement throughout is low. A 90° *Horace* scan was taken with 0. 5° steps and ~13 minutes of counting per step (~8 μA h). The *Mantid* software was used for data normalization, and the *Horace* package was used to construct four-dimensional $S(\mathbf{Q}, \omega)$ datasets[61,62].

Data availability

Professor Geetha Balakrishnan et al. (2023): Magnon Dispersions in the Centrosymmetric Skyrmion Host GdRu2Si2, STFC ISIS Neutron and Muon Source, https://doi.org/10.5286/ISIS.E.RB2310357. Analysis code is available on request from the corresponding author.

Received: 10 December 2024; Accepted: 23 March 2025;
Published online: 16 April 2025

References

1. He, Q. L., Hughes, T. L., Armitage, N. P., Tokura, Y. & Wang, K. L. Topological spintronics and magnetoelectronics. *Nat. Mater.* **21**, 15–23 (2022).
2. Fert, A., Reyren, N. & Cros, V. Magnetic skyrmions: advances in physics and potential applications. *Nat. Rev. Mater.* **2**, 17031 (2017).
3. Lancaster, T. Skyrmions in magnetic materials. *Contemp. Phys.* **60**, 246–261 (2019).
4. Tokura, Y. & Kanazawa, N. Magnetic skyrmion materials. *Chem. Rev.* **121**, 2857–2897 (2020).
5. Wang, Z., Su, Y., Lin, S.-Z. & Batista, C. D. Meron, skyrmion, and vortex crystals in centrosymmetric tetragonal magnets. *Phys. Rev. B* **103**, 104408 (2021).
6. Hayami, S. Zero-field skyrmion, meron, and vortex crystals in centrosymmetric hexagonal magnets. *J. Magn. Magn. Mater.* **564**, 170036 (2022).
7. Yu, X. et al. Magnetic stripes and skyrmions with helicity reversals. *Proc. Natl Acad. Sci.* **109**, 8856–8860 (2012).
8. Yao, X., Chen, J. & Dong, S. Controlling the helicity of magnetic skyrmions by electrical field in frustrated magnets. *N. J. Phys.* **22**, 083032 (2020).
9. Yao, X. & Dong, S. Vector vorticity of skyrmionic texture: An internal degree of freedom tunable by magnetic field. *Phys. Rev. B* **105**, 014444 (2022).
10. Kurumaji, T. et al. Skyrmion lattice with a giant topological Hall effect in a frustrated triangular-lattice magnet. *Science* **365**, 914–918 (2019).
11. Paddison, J. A. M. et al. Magnetic interactions of the centrosymmetric skyrmion material Gd_2PdSi_3. *Phys. Rev. Lett.* **129**, 137202 (2022).
12. Ju, J. et al. Polarized neutron scattering study of the centrosymmetric skyrmion host material Gd_2PdSi_3. *Phys. Rev. B* **107**, 024405 (2023).
13. Hirschberger, M. et al. Skyrmion phase and competing magnetic orders on a breathing kagomé lattice. *Nat. Commun.* **10**, 5831 (2019).
14. Hirschberger, M. et al. Lattice-commensurate skyrmion texture in a centrosymmetric breathing kagome magnet. *npj Quantum Mater.* **9**, 45 (2024).
15. Khanh, N. D. et al. Nanometric square skyrmion lattice in a centrosymmetric tetragonal magnet. *Nat. Nanotechnol.* **15**, 444–449 (2020).
16. Yasui, Y. et al. Imaging the coupling between itinerant electrons and localised moments in the centrosymmetric skyrmion magnet $GdRu_2Si_2$. *Nat. Commun.* **11**, 5925 (2020).
17. Utesov, O. I. Thermodynamically stable skyrmion lattice in a tetragonal frustrated antiferromagnet with dipolar interaction. *Phys. Rev. B* **103**, 064414 (2021).
18. Khanh, N. D. et al. Zoology of multiple-Q spin textures in a centrosymmetric tetragonal magnet with itinerant electrons. *Adv. Sci.* **9**, 2105452 (2022).
19. Wood, G. D. A. et al. Double-Q ground state with topological charge stripes in the centrosymmetric skyrmion candidate $GdRu_2Si_2$. *Phys. Rev. B* **107**, L180402 (2023).
20. Spethmann, J. et al. SP-STM study of the multi-Q phases in $GdRu_2Si_2$. *Phys. Rev. Mater.* **8**, 064404 (2024).
21. Huddart, B. M. et al. Field-orientation-dependent magnetic phases in $GdRu_2Si_2$ probed with muon-spin spectroscopy. *Phys. Rev. B* **111**, 054440 (2025).
22. Yoshimochi, H. et al. Multistep topological transitions among meron and skyrmion crystals in a centrosymmetric magnet. *Nat. Phys.* **20**, 1001–1008 (2024).
23. Meier, W. R. et al. Thermodynamic insights into the intricate magnetic phase diagram of $EuAl_4$. *Phys. Rev. B* **106**, 094421 (2022).
24. Takagi, R. et al. Square and rhombic lattices of magnetic skyrmions in a centrosymmetric binary compound. *Nat. Commun.* **13**, 1472 (2022).
25. Hayami, S. Orthorhombic distortion and rectangular skyrmion crystal in a centrosymmetric tetragonal host. *J. Phys.: Mater.* **6**, 014006 (2022).
26. Gen, M. et al. Rhombic skyrmion lattice coupled with orthorhombic structural distortion in $EuAl_4$. *Phys. Rev. B* **107**, L020410 (2023).
27. Vibhakar, A. M. et al. Spontaneous reversal of spin chirality and competing phases in the topological magnet $EuAl_4$. *Commun. Phys.* **7**, 313 (2024).
28. Moya, J. M. et al. Incommensurate magnetic orders and topological Hall effect in the square-net centrosymmetric $EuGa_2Al_2$ system. *Phys. Rev. Mater.* **6**, 074201 (2022).

29. Vibhakar, A. M. et al. Competing charge and magnetic order in the candidate centrosymmetric skyrmion host $EuGa_2Al_2$. *Phys. Rev. B* **108**, L100404 (2023).
30. Littlehales, M. T. et al. Spin density waves and ground state helices in $EuGa_{2.4}Al_{1.6}$. *Phys. Rev. Res.* **6**, L032015 (2024).
31. Shatruk, M. $ThCr_2Si_2$ structure type: The "perovskite" of intermetallics. *J. Solid State Chem.* **272**, 198–209 (2019).
32. Nomoto, T. & Arita, R. Ab initio exploration of short-pitch skyrmion materials: Role of orbital frustration. *J. Appl. Phys.* **133**, 150901 (2023).
33. Bouaziz, J., Mendive-Tapia, E., Blügel, S. & Staunton, J. B. Fermi-surface origin of skyrmion lattices in centrosymmetric rare-earth intermetallics. *Phys. Rev. Lett.* **128**, 157206 (2022).
34. Andriushin, N. et al. Reentrant multiple-**q** magnetic order and a "spin meta-cholesteric" phase in $Sr_3Fe_2O_7$. *npj Quantum Mater.* **9**, 84 (2024).
35. Puphal, P. et al. Topological magnetic phase in the candidate Weyl semimetal CeAlGe. *Phys. Rev. Lett.* **124**, 017202 (2020).
36. Luttinger, J. & Tisza, L. Theory of dipole interaction in crystals. *Phys. Rev.* **70**, 954 (1946).
37. Lyons, D. & Kaplan, T. Method for determining ground-state spin configurations. *Phys. Rev.* **120**, 1580 (1960).
38. Kurz, P., Bihlmayer, G., Hirai, K. & Blügel, S. Three-dimensional spin structure on a two-dimensional lattice: Mn/Cu (111). *Phys. Rev. Lett.* **86**, 1106 (2001).
39. Garnier, A., Gignoux, D., Schmitt, D. & Shigeoka, T. Giant magnetic anisotropy in tetragonal $GdRu_2Ge_2$ and $GdRu_2Si_2$. *Phys. B: Condens. Matter* **222**, 80–86 (1996).
40. Janoschek, M. et al. Helimagnon bands as universal excitations of chiral magnets. *Phys. Rev. B* **81**, 214436 (2010).
41. Kugler, M. et al. Band structure of helimagnons in MnSi resolved by inelastic neutron scattering. *Phys. Rev. Lett.* **115**, 097203 (2015).
42. Portnichenko, P. et al. Magnon spectrum of the helimagnetic insulator Cu_2OSeO_3. *Nat. Commun.* **7**, 10725 (2016).
43. Balz, C. et al. Magnetic Hamiltonian and phase diagram of the quantum spin liquid $Ca_{10}Cr_7O_{28}$. *Phys. Rev. B* **95**, 174414 (2017).
44. Paddison, J. A. M. et al. Continuous excitations of the triangular-lattice quantum spin liquid $YbMgGaO_4$. *Nat. Phys.* **13**, 117–122 (2017).
45. Boothroyd, A. T. *Principles of Neutron Scattering from Condensed Matter* (Oxford University Press, 2020). https://doi.org/10.1093/oso/9780198862314.001.0001.
46. Lovesey, S. W. *Theory of neutron scattering from condensed matter*, vol. 2 (Oxford University Press, 1984).
47. Newville, M. et al. LMFIT: Non-linear least-square minimization and curve-fitting for Python https://doi.org/10.5281/zenodo.11813 (2015).
48. Zhang, H. & Batista, C. D. Classical spin dynamics based on SU(N) coherent states. *Phys. Rev. B* **104**, 104409 (2021).
49. Dahlbom, D. et al. Geometric integration of classical spin dynamics via a mean-field Schrödinger equation. *Phys. Rev. B* **106**, 054423 (2022).
50. McClarty, P. et al. Chain-based order and quantum spin liquids in dipolar spin ice. *Phys. Rev. B* **92**, 094418 (2015).
51. den Hertog, B. C. & Gingras, M. J. Dipolar interactions and origin of spin ice in ising pyrochlore magnets. *Phys. Rev. Lett.* **84**, 3430 (2000).
52. Paddison, J. A. M. et al. Spin dynamics of the centrosymmetric skyrmion material $GdRu_2Si_2$. *Cell Rep. Phys. Sci.* **5**, 102280 (2024).
53. Eremeev, S. et al. Insight into the electronic structure of the centrosymmetric skyrmion magnet $GdRu_2Si_2$. *Nanoscale Adv.* **5**, 6678–6687 (2023).
54. Dong, Y. et al. Magnetic-domain-dependent pseudogap induced by Fermi surface nesting in a centrosymmetric skyrmion magnet. arXiv preprint arXiv:2307.08000 https://doi.org/10.48550/arXiv.2307.08000 (2023).
55. Matsuyama, N. et al. Quantum oscillations in the centrosymmetric skyrmion-hosting magnet $GdRu_2Si_2$. *Phys. Rev. B* **107**, 104421 (2023).
56. Zaliznyak, I. A. Spiral order induced by distortion in a frustrated square-lattice antiferromagnet. *Phys. Rev. B* **69**, 092404 (2004).
57. Zaliznyak, I. A. Heisenberg magnet with modulated exchange. *Phys. Rev. B* **68**, 134451 (2003).
58. Korshunov, A. et al. Phonon softening and atomic modulations in $EuAl_4$. *Phys. Rev. B* **110**, 045102 (2024).
59. Ni, H. et al. Real-space visualization of atomic displacements in a long-wavelength charge density wave using cryogenic 4D-stem. *Phys. Rev. Mater.* **8**, 104414 (2024).
60. Bewley, R., Taylor, J. & Bennington, S. LET, a cold neutron multi-disk chopper spectrometer at ISIS. *Nucl. Instrum. Methods Phys. Res. A: Accel Spectrom. Detect. Associat. Equip.* **637**, 128–134 (2011).
61. Arnold, O. et al. MANTID-Data analysis and visualization package for neutron scattering and μSR experiments. *Nucl. Instrum. Methods Phys. Res. A: Accel Spectrom. Detect. Associat. Equip.* **764**, 156–166 (2014).
62. Ewings, R. et al. HORACE: Software for the analysis of data from single crystal spectroscopy experiments at time-of-flight neutron instruments. *Nucl. Instrum. Methods Phys. Res. A: Accel Spectrom. Detect. Associat. Equip.* **834**, 132–142 (2016).

Acknowledgements

We are grateful for the useful discussions with Jacob Wilkins (Scientific Computing Department, STFC), Manh Duc Le, Toby Perring, Travis Williams, David Voneshen (ISIS Neutron and Muon Source, STFC), and Harry Lane (University of Manchester). The work of J. A. M. P. was supported by the U.S. Department of Energy, Office of Science, Basic Energy Sciences, Materials Sciences and Engineering Division. This paper was financially supported by two Engineering and Physical Sciences Research Council grants: EP/T005963/1, the UK Skyrmion Project, EP/N032128/1 and by the U.K. Research and Innovation and Science and Technology Facilities Council through the provision of beam time at the ISIS Neutron and Muon Source, as well as partial funding for the ^{160}Gd isotope. The ^{160}Gd isotope was procured from the National Isotope Development Center, Oak Ridge National Laboratory, USA.

Author contributions

G.D.A.W., G.B., S.M.T., O.A.P., and J.R.S. conceived the experiment. D.A.M. and G.B. performed the crystal growth. G.D.A.W., J.R.S., and S.M.T. performed the LET experiment. G.D.A.W and M.R.L performed the magnetometry. J.B. and J.B.S. provided theoretical calculations. G.D.A.W. analysed the experiment with advice from J.A.M.P., J.R.S, J.B.S., and P.M. G.D.A.W. wrote the manuscript and the co-authors reviewed it.

Competing interests

The authors declare no competing interests.

Additional information

Supplementary information The online version contains supplementary material available at https://doi.org/10.1038/s41535-025-00755-6.

Correspondence and requests for materials should be addressed to G. D. A. Wood or G. Balakrishnan.